Effect of regularization of Schmid law on self-consistent estimates for rate-independent plasticity of polycrystals

Kengo Yoshida, Renald Brenner, Brigitte Bacroix, Salima Bouvier

Accepted Manuscript

Please cite this article as: Yoshida, K., Brenner, R., Bacroix, B., Bouvier, S. Effect of regularization of Schmid law on self-consistent estimates for rate-independent plasticity of polycrystals, European Journal of Mechanics / A Solids (2009), doi: 10.1016/j.euromechsol.2009.05.001

This is a PDF file of an unedited manuscript that has been accepted for publication. As a service to our customers we are providing this early version of the manuscript. The manuscript will undergo copyediting, typesetting, and review of the resulting proof before it is published in its final form. Please note that during the production process errors may be discovered which could affect the content, and all legal disclaimers that apply to the journal pertain.

Effect of regularization of Schmid law on self-consistent estimates for rate-independent plasticity of polycrystals

Kengo Yoshida[a,b*], Renald Brenner[a], Brigitte Bacroix[a] and Salima Bouvier[a]

[a] LPMTM, CNRS, University Paris 13, 99 Avenue Jean-Baptiste Clement, 93430 Villetaneuse, France

[b] Forming Technologies R&D Center, Steel Research Laboratories, Nippon Steel Corporation, 20-1 Shintomi, Futtsu, Chiba 293-8511, Japan

*Corresponding author

Tel.: +33 1 49 40 34 67;   Fax: +33 1 49 40 39 38.

E-mail address: yoshida.kengo1@nsc.co.jp (K. Yoshida).

Abstract

The mechanical response of an elastoplastic polycrystalline aggregate is estimated by means of Taylor and Hill's incremental self-consistent models in conjunction with two rate-independent crystal plasticity laws: standard and regularized Schmid laws. With the Taylor model, both constitutive laws lead to the same result whereas for the self-consistent model, the standard Schmid law predicts softer effective response than the regularized Schmid law and higher strain heterogeneity within the polycrystal. It is found that these features are related to the decrease of the shear tangent moduli during deformation when the standard Schmid law is considered. The presented results with the regularized Schmid law are in agreement with previous findings for power law viscoplastic polycrystals. It is demonstrated that the description of the crystal plasticity law significantly affects the estimate delivered by the Hill's incremental self-consistent model for elastoplastic polycrystals.

Keywords

1. Introduction

Homogenization methods are efficient approaches to estimate the mechanical properties of heterogeneous materials. In the case of polycrystalline media, theoretical results have shown that the linear elastic self-consistent model (Hershey, 1954; Kröner, 1958) is well appropriated to describe their effective properties (Kröner, 1978). This has been assessed by comparing the effective behavior and the local fields with results delivered by full-field computations on various polycrystalline microstructures (see, for instance, Lebensohn et al., 2004; Castelnau et al., 2006; Brenner et al., submitted).

The extension of the self-consistent model to rate-independent elastoplastic behavior has first been proposed by Budiansky et al. (1960) and Kröner (1961) who investigated the early stage of plasticity by considering plastic grains interacting with an elastic matrix. To describe entirely the elastoplastic response of polycrystals, a seminal work was further introduced by Hill (1965) and Hutchinson (1970) who proposed an incremental approach based on the linear rate-form of local constitutive equations which rely on the Schmid law. More recently, an affine approach has been proposed by Masson et al. (2000) who showed, for a non-hardening f.c.c. polycrystal, that it leads to a lower steady-state effective yield stress than the incremental model.

In the related context of power-law viscoplastic f.c.c. polycrystals, various extensions of the self-consistent model, including the incremental (Hutchinson, 1976) and affine (Masson et al, 2000) approaches, have been compared to rigorous nonlinear bounds obtained with the variational procedure of Ponte Castañeda (1991). Nebozhyn et al. (2001) have shown that the incremental model violates the variational self-consistent estimate on the effective yield stress, which is an upper bound for all self-consistnet estimates, and tends to the Taylor bound in the rate-independent limit. By contrast, the affine model respects the available bounds, for this specific class of polycrystals. In view of these results, Hill's incremental model (1965) could be expected to present similar shortcomings in the context of rate-independent elastoplasticity. However, a few works (Hutchinson, 1970 and Takahashi, 1988) show that the incremental model estimates softer response than the Taylor bound for elastoplasticity, which contradicts

61　the above expectation. The link between the rate-independent limit of viscoplasticity and

62　rate-independent elastoplasticity remains an open question.

63

64　In the present work, we analyze the influence of the local elastoplastic behavior on the

65　incremental self-consistent estimate of the polycrystal response. For that goal, two

66　rate-independent crystal plasticity models have been chosen. On one hand, use is made of the

67　Standard Schmid Law (SSL) in which plastic slip is considered to occur on a slip system

68　when the resolved shear stress reaches a critical value. This constitutive law leads multi-yield

69　functions and the determination of the slip rates is an inverse problem of the constraint

70　conditions. The constraints can be linearly dependent and result in the non-uniqueness of the

71　set of active slip systems when the hardening matrix is not positive definite (Hill, 1966). This

72　has led to various proposals for the hardening description (see, for instance, Franciosi and

73　Zaoui, 1991; Bassani, 1994) and for the technique to identify the set of slip systems (Anand

74　and Kothari, 1996; Miehe and Schröder, 2001; Busso and Cailletaud, 2005). A simple and

75　often used method to circumvent this difficulty is to forsake the rate-independent formulation

76　and adopt a power-law type rate-dependent viscoplastic formulation (see, for instance, Asaro

77　and Needleman, 1985). On the other hand, Regularized Schmid Law (RSL) has been

78　proposed to overcome this problem within the framework of the rate-independent plasticity

79　(see, Gambin, 1992; Darrieulat and Piot, 1996; Franz et al. 2009). The advantage of the

80　regularization is that it does not involve the problem of linear dependence. It has been used in

81　the homogenization context with the Taylor model (Darrieulat and Piot, 1996, Kowalczyk and

82　Gambin, 2004), the Transformation Field Analysis (Franciosi and Berbenni, 2007) and,

83　recently, the self-consistent model (Franz et al. 2009). In section 2, two crystal-plasticity

84　models (SSL and RSL) are presented and the corresponding tangent moduli in the rate-form

85　constitutive relations are compared for single and double slip cases in the single crystal

86　context. These crystal plasticity laws are then introduced in the Taylor and incremental

87　self-consistent models and the mechanical responses of two different non-hardening f.c.c.

88　polycrystals are estimated (Sections 3 and 4). The significance of the description of

89　constitutive law, especially the instantaneous tangent moduli, on the self-consistent estimates

90　is discussed in details in section 5.

91

2. Rate-independent crystal plasticity models

2.1. Framework of crystal plasticity model

In this study, we confine attention to small strain conditions. The strain rate is given by the symmetry part of $\partial \mathbf{v} / \partial \mathbf{x}$, where $\mathbf{v}$ and $\mathbf{x}$ are velocity and position, respectively. We consider additive decomposition of strain rate into elastic and plastic parts.

$$\dot{\boldsymbol{\varepsilon}} = \dot{\boldsymbol{\varepsilon}}^{e} + \dot{\boldsymbol{\varepsilon}}^{p}. \tag{1}$$

Elastic relation is given by Hooke's law.

$$\dot{\boldsymbol{\sigma}} = \mathbf{C}^{e} : \dot{\boldsymbol{\varepsilon}}^{e} = \mathbf{C}^{e} : (\dot{\boldsymbol{\varepsilon}} - \dot{\boldsymbol{\varepsilon}}^{p}), \tag{2}$$

where $\mathbf{C}^{e}$ is the forth-order elastic moduli tensor.

101

Crystallographic slips are considered to be the source for the plastic deformation, and the plastic strain rate takes the form

$$\dot{\boldsymbol{\varepsilon}}^{p} = \sum_{\alpha} \dot{\gamma}^{(\alpha)} \mathbf{p}^{(\alpha)}, \tag{3}$$

$$\mathbf{p}^{(\alpha)} := \frac{1}{2} (\mathbf{s}^{(\alpha)} \otimes \mathbf{m}^{(\alpha)} + \mathbf{m}^{(\alpha)} \otimes \mathbf{s}^{(\alpha)}), \tag{4}$$

where $\dot{\gamma}^{(\alpha)}$, $\mathbf{s}^{(\alpha)}$ and $\mathbf{m}^{(\alpha)}$ are the slip rate, the slip direction and the slip plane normal for the α th slip system, respectively. The resolved shear stress for the α th slip system, $\tau^{(\alpha)}$, is written as

$$\tau^{(\alpha)} = \mathbf{s}^{(\alpha)} \cdot \boldsymbol{\sigma} \cdot \mathbf{m}^{(\alpha)} = \boldsymbol{\sigma} : \mathbf{p}^{(\alpha)}, \tag{5}$$

where $\boldsymbol{\sigma}$ is true stress. From Equations (3) and (5), a resolved shear stress rate is given as

$$\dot{\tau}^{(\alpha)} = \mathbf{p}^{(\alpha)} : \mathbf{C}^{e} : \dot{\boldsymbol{\varepsilon}} - \sum_{\beta} \dot{\gamma}^{(\beta)} \mathbf{p}^{(\alpha)} : \mathbf{C}^{e} : \mathbf{p}^{(\beta)}, \tag{6}$$

where $\mathbf{s}^{(\alpha)}$ and $\mathbf{m}^{(\alpha)}$ are assumed to be constant. Slip resistance for the α th slip system is denoted by $g^{(\alpha)}$, and its evolution is governed by

114
$$\dot{g}^{(\alpha)} = \sum_{\beta} h^{\alpha\beta} \mid \dot{\gamma}^{(\beta)} \mid, \tag{7}$$

115   where $h^{\alpha\beta}$ denotes hardening moduli.

116

117   *2.2. Standard Schmid law*

118   For a crystal plasticity model based on the standard Schmid law, the local yield function, f,

119   is written as

120
$$f = \sup_{\alpha=1,\cdots,N^s} f^{(\alpha)} = 0, \tag{8}$$

121   with

122
$$f^{(\alpha)} = \mid \tau^{(\alpha)} \mid - g^{(\alpha)} = 0, \tag{9}$$

123   where N^s is the number of slip systems and $f^{(\alpha)}$ is a yield function for each slip system.

124   The plastic strain rate is given by

125
$$\dot{\boldsymbol{\varepsilon}}^p = \sum_{\alpha} \operatorname{sgn}(\tau^{(\alpha)}) \dot{\gamma}^{(\alpha)} \mathbf{p}^{(\alpha)}, \tag{10}$$

126   where slip rates, $\dot{\gamma}^{(\alpha)}$, are assumed to be positive. It is worth noting that the above equation

127   can be derived from the normality rule if the yield function for each slip system is considered

128   as a potential: $\dot{\boldsymbol{\varepsilon}}^p = \sum_{\alpha} \dot{\gamma}^{(\alpha)} (\partial f^{(\alpha)} / \partial \boldsymbol{\sigma})$.

129

130   Based on N^s independent yield functions (Equation (9)) potentially active and inactive slip

131   systems are classified as

132
$$\dot{\gamma}^{(\alpha)} \geq 0, \quad \text{for} \ \ f^{(\alpha)} = 0 \ \ \text{and} \ \ \dot{f}^{(\alpha)} = 0, \tag{11a}$$

133
$$\dot{\gamma}^{(\alpha)} = 0, \quad \text{for} \ \ f^{(\alpha)} < 0, \text{or} \ \ f^{(\alpha)} = 0 \ \ \text{and} \ \ \dot{f}^{(\alpha)} < 0. \tag{11b}$$

134   From the consistency condition of the yield functions, the slip rates, $\dot{\gamma}^{(\alpha)}$, on the active slip

135   systems are determined as

136
$$\dot{f}^{(\alpha)} = R^{\alpha} - \sum_{\beta} X^{\alpha\beta} \dot{\gamma}^{(\beta)} = 0, \tag{12}$$

137 $$\dot{\gamma}^{(\alpha)} = \sum_{\beta} Y^{\alpha\beta} R^{(\beta)} \; ,$$ (13)

138 where

139 $$R^{(\alpha)} := \mathrm{sgn}(\tau^{(\alpha)})\mathbf{p}^{(\alpha)} : \mathbf{C}^{\mathrm{e}} : \dot{\boldsymbol{\varepsilon}} ,$$ (14a)

140 $$X^{\alpha\beta} := h^{\alpha\beta} + \mathrm{sgn}(\tau^{(\alpha)})\,\mathrm{sgn}(\tau^{(\beta)})\mathbf{p}^{(\alpha)} : \mathbf{C}^{\mathrm{e}} : \mathbf{p}^{(\beta)} ,$$ (14b)

141 $$[Y^{\alpha\beta}] := [X^{\alpha\beta}]^{-1} ,$$ (14c)

142 where $(\bullet)^{-1}$ denotes the inverse. Under a particular hardening rule, $h^{\alpha\beta}$, $X^{\alpha\beta}$ may become

143 singular, and this results in a possible non-uniquess of the set of the active slip systems for a

144 given deformation mode. But for perfect plasticity, $h^{\alpha\beta} = 0$, it is always possible to choose at

145 least one set of linearly independent slip systems from the potentially active slip systems such

146 that $X^{\alpha\beta}$ is non-singular and Equations (11) are satisfied (Hutchinson, 1970). If there are

147 greater than five linearly independent systems, five slip systems are selected in the

148 computations[1].

149

150 Using equations (2), (10) and (13), we finally obtain the rate-form of the constitutive

151 equation, $\dot{\boldsymbol{\sigma}} = \mathbf{L} : \dot{\boldsymbol{\varepsilon}}$, in term of the elastoplastic tangent moduli,

152 $$\mathbf{L} := \mathbf{C}^{\mathrm{e}} - \sum_{\alpha} \left\{ \left(\mathrm{sgn}(\tau^{(\alpha)})\mathbf{C}^{\mathrm{e}} : \mathbf{p}^{(\alpha)} \right) \otimes \sum_{\beta} \left(\mathrm{sgn}(\tau^{(\beta)})Y^{\alpha\beta}\mathbf{p}^{(\beta)} : \mathbf{C}^{\mathrm{e}} \right) \right\} .$$ (15)

153

154 *2.3. Regularized Schmid law*

155 In order to avoid the possible singularity of $X^{\alpha\beta}$ in the Schmid law, a regularized Schmid

156 law for rate-independent crystal plasticity was proposed (Gambin, 1992). The following

---

[1] For comparison purpose we use the same approach as Hutchinson's (1970). In a preliminary

study, different criteria have been used for the selection of the five active slip systems, and it

has been confirmed that the choice of the criterion does not have any influence on the

estimation.

157   regularized yield function is introduced.

158    $$f = \left\{ \sum_{\alpha} \left(\frac{\tau^{(\alpha)}}{g^{(\alpha)}} \right)^{2N} \right\}^{\frac{1}{2N}} - 1 = 0 ,$$ (16)

159   where N is an integer parameter so that the exponent always becomes an even number. The

160   plastic strain rate is assumed to be given by

161    $$\dot{\boldsymbol{\varepsilon}}^{\mathrm{p}} = \sum_{\alpha} \dot{\gamma}^{(\alpha)} \mathbf{p}^{(\alpha)} ,$$ (17)

162   and follows, on the other hand, from the normality rule associated with the yield function

163   (16),

164    $$\dot{\boldsymbol{\varepsilon}}^{\mathrm{p}} = \dot{\Lambda} \frac{\partial f}{\partial \boldsymbol{\sigma}} .$$ (18)

165   From these two expressions of the plastic strain rate, the slip rate on a given slip system reads

166    $$\dot{\gamma}^{(\alpha)} = \frac{\dot{\lambda}}{g^{(\alpha)}} \left(\frac{\tau^{(\alpha)}}{g^{(\alpha)}} \right)^{2N-1} \quad \text{with} \quad \dot{\lambda} = \dot{\Lambda} \left\{ \sum_{\alpha} \left(\frac{\tau^{(\alpha)}}{g^{(\alpha)}} \right)^{2N} \right\}^{\frac{1}{2N}-1} ,$$ (19)

167   where $\dot{\lambda}$ is a positive plastic multiplier. By contrast to the SSL, slip rates for all the slip

168   systems derived from a unique plastic multiplier. Therefore, there is no need to classify active

169   and inactive slip systems among the set of slip systems. Equation (19) is similar to the one

170   describing vicsoplastic crystal (e.g. Asaro and Needleman, 1985) in which a reference slip

171   rate is introduced instead of a plastic multiplier.

172

173   Loading-unloading conditions are written as

174    $$\dot{\lambda} \geq 0 , \quad \text{for} \ f = 0 \ \text{and} \ \dot{f} = 0 ,$$ (20a)

175    $$\dot{\lambda} = 0 , \quad \text{for} \ f < 0 , \text{or} \ f = 0 \ \text{and} \ \dot{f} < 0 .$$ (20b)

176   From the consistency condition of the yield function, the plastic multiplier, $\dot{\lambda}$, is determined.

177    $$\dot{f} = \mathbf{G} : \mathbf{C}^{\mathrm{e}} : \dot{\boldsymbol{\varepsilon}} - \dot{\lambda} (\mathbf{G} : \mathbf{C}^{\mathrm{e}} : \mathbf{G} + H) = 0 ,$$ (21)

178
$$\dot{\lambda} = \frac{\mathbf{G} : \mathbf{C}^e : \dot{\boldsymbol{\varepsilon}}}{\mathbf{G} : \mathbf{C}^e : \mathbf{G} + H}, \tag{22}$$

179 where

180
$$\mathbf{G} := \sum_{\alpha} \left\{ \left(\frac{\tau^{(\alpha)}}{g^{(\alpha)}} \right)^{2N-1} \frac{\mathbf{p}^{(\alpha)}}{g^{(\alpha)}} \right\}, \tag{23a}$$

181
$$H := \sum_{\alpha} \left[\left(\frac{\tau^{(\alpha)}}{g^{(\alpha)}} \right)^{2N} \frac{1}{g^{(\alpha)}} \sum_{\beta} \left\{ \frac{h_{\alpha\beta}}{g^{(\beta)}} \left(\frac{|\tau^{(\beta)}|}{g^{(\beta)}} \right)^{2N-1} \right\} \right]. \tag{23b}$$

182 In the derivation of $\dot{\lambda}$, any inverse of a matrix is not required. Namely, the difficulty related

183 to the linearly dependence in the Schmid law is avoided.

184

185 We finally obtain the rate-form constitutive equation for a single crystal, $\dot{\boldsymbol{\sigma}} = \mathbf{L} : \dot{\boldsymbol{\varepsilon}}$, in terms of

186 the elastoplastic tangent moduli,

187
$$\mathbf{L} := \mathbf{C}^e - \frac{(\mathbf{C}^e : \mathbf{G}) \otimes (\mathbf{G} : \mathbf{C}^e)}{\mathbf{G} : \mathbf{C}^e : \mathbf{G} + H}. \tag{24}$$

188

189 *2.3. Comparison of Schmid and regularized Schmid laws*

190 In this subsection, the standard Schmid and regularized Schmid laws are compared in terms of

191 yield locus, active slip systems and tangent moduli. The SSL gives multi-plane yield locus

192 which possesses corners, while the RSL gives a smooth yield locus with rounded corners. The

193 curvature of the rounded corner for the RSL increases with the exponent N, and when N is

194 large enough, the smooth yield locus is in good agreement with the multi-plane SSL's one

195 (Darrieulat and Piot, 1996; Gambin and Barlat, 1997). Besides, although all the slip systems

196 are active if the yield condition is satisfied, finite slips take place only on the slip systems

197 where $\tau^{(\alpha)} \approx g^{(\alpha)}$ when the exponent N is large, while slip rates for the other slip systems,

198 where $\tau^{(\alpha)} < g^{(\alpha)}$, are close to zero (Equation (19)). This is similar to the Schmid law, for

199 which slip system activates when $\tau^{(\alpha)} = g^{(\alpha)}$. Therefore, the yield locus and active slip

200 systems corresponding to the Schmid law are correctly described by the regularized Schmid

201 law when $N \to +\infty$. On the contrary, the tangent moduli given in Equation (15) and (24) are

202 not identical a priori. To be more specific, the tangent moduli given by the two laws are

203 compared for some special cases.

204

205   *(i) Single slip case*

206   Let us consider a crystal that possesses a single slip system. The exponent in the regularized

207   Schmid law is taken to $N = +\infty$. In this case, the yield function (16) reduces to Equation (9).

208   It is assumed that $\tau^{(1)} = g^{(1)}$ and $\dot{\tau}^{(1)} = \dot{g}^{(1)}$ for the slip system. This situation results in the

209   activation of the slip system for both SSL and RSL. Then the tangent moduli is written as

210
$$\mathbf{L} = \mathbf{C}^{e} - \frac{(\mathbf{C}^{e} : \mathbf{p}^{(1)}) \otimes (\mathbf{p}^{(1)} : \mathbf{C}^{e})}{\mathbf{p}^{(1)} : \mathbf{C}^{e} : \mathbf{p}^{(1)} + h^{11}} . \tag{25}$$

211   The tangent moduli (15) and (24) are reduced to the same equation.

212

213   *(ii) Double slip case*

214   Next, let us consider a crystal that possesses two slip systems. It is assumed that $\tau^{(1)} = g^{(1)}$,

215     $\tau^{(2)} = g^{(2)}$ and $\dot{\tau}^{(1)} = \dot{g}^{(1)}$, $\dot{\tau}^{(2)} = \dot{g}^{(2)}$. For both the Schmid and regularized Schmid laws, the

216   yield criteria are satisfied and slips occur for both the first and second slip systems. These

217   situations are similar to that for the single slip case. In this case, the tangent moduli obtained

218   with the Schmid law (Equation(15)) reduces to

219
$$\mathbf{L} = \mathbf{C}^{e} - \mathbf{C}^{e} : \{\mathbf{p}^{(1)} \otimes (Y^{11}\mathbf{p}^{(1)} + Y^{12}\mathbf{p}^{(2)}) + \mathbf{p}^{(2)} \otimes (Y^{21}\mathbf{p}^{(1)} + Y^{22}\mathbf{p}^{(2)})\} : \mathbf{C}^{e}, \tag{26}$$

220   where

221
$$\begin{bmatrix} Y^{11} & Y^{12} \\ Y^{21} & Y^{22} \end{bmatrix} = \begin{bmatrix} h^{11} + \mathbf{p}^{(1)} : \mathbf{C}^{e} : \mathbf{p}^{(1)} & h^{12} + \mathbf{p}^{(1)} : \mathbf{C}^{e} : \mathbf{p}^{(2)} \\ h^{21} + \mathbf{p}^{(2)} : \mathbf{C}^{e} : \mathbf{p}^{(1)} & h^{22} + \mathbf{p}^{(2)} : \mathbf{C}^{e} : \mathbf{p}^{(2)} \end{bmatrix}^{-1} , \tag{27}$$

222   and $g^{(1)} = g^{(2)}$ is assumed for simplicity.

223

224   With the regularized Schmid law, the tangent moduli (Equation(24)) gives

225
$$\mathbf{L} = \mathbf{C}^{e} - \frac{\mathbf{C}^{e} : (\mathbf{p}^{(1)} + \mathbf{p}^{(2)}) \otimes (\mathbf{p}^{(1)} + \mathbf{p}^{(2)}) : \mathbf{C}^{e}}{(\mathbf{p}^{(1)} + \mathbf{p}^{(2)}) : \mathbf{C}^{e} : (\mathbf{p}^{(1)} + \mathbf{p}^{(2)}) + h_{11} + h_{12} + h_{21} + h_{22}} . \tag{28}$$

226   For the double slip case, the two crystal plasticity laws do not give the identical expression of

227   tangent moduli. For the Schmid law, interaction of $\mathbf{p}^{(\alpha)}$ for each slip system appears with

228   different coefficient, $Y^{\alpha\beta}$, while interaction of the summation of $\mathbf{p}^{(\alpha)}$ emerges for the

229   regularized Schmid law.

230

231   The tangent moduli given by the two laws are calculated for a special case shown in Figure 1

232   (a). Two slip systems are arranged symmetrically about the x_1 axis and slip directions and

233   slip plane normals are in the $x_1 - x_2$ plane, that is,

234    $\mathbf{s}^{(1)} = (\cos\phi, \sin\phi, 0)$ $\mathbf{m}^{(1)} = (\sin\phi, -\cos\phi, 0)$, $\mathbf{s}^{(2)} = (\cos\phi, -\sin\phi, 0)$ and

235    $\mathbf{m}^{(2)} = (\sin\phi, \cos\phi, 0)$. For simplicity, isotropic elasticity and non-hardening is assumed.

236   Then, analytical expression of tangent moduli are written as

237    $$L_{1111} = L_{2222} = L_{1122} = \lambda + \mu,$$ (29a)

238    $$L_{1212} = \begin{cases} C^e_{1212} - \mu = 0 & \text{for the Schmid law} \\ C^e_{1212} = \mu & \text{for the regularized Schmid law} \end{cases}$$ (29b)

239    $$L_{ijkl} = C^e_{ijkl} \quad \text{for others components}$$ (29c)

240   where λ and μ are Lamé constants. The difference of tangent modulus is appeared for

241   L_{1212} component.

242

243   In the derivation of the analytical expression of the tangent moduli $N = +\infty$ is assumed,

244   however, a finite value of N is required in actual computation. In order to check the

245   sensitivity of N, the same problem is solved numerically with $N = 500$. Parameters are set

246   to $\phi = 15°$, $E/\tau_0 = 1000$, $\nu = 1/3$ and $h^{\alpha\beta} = 0$, where E, ν and τ_0 are the Young's

247   modulus, Poisson's ratio and critical resolved shear stress, respectively. Uniaxial tension in

248   the x_1 direction is applied. Figure 1(b) shows the tangent moduli normalized by E as a

249   function of the tensile strain. Tangent moduli given by the two crystal plasticity laws coincide

250   except for the L_{1212} component, and L_{1212} for the Schmid law decrease to zero when the

251   yield condition is satisfied, whereas that for the regularized Schmid law remains constant. The

252   tangent moduli computed with $N = 500$ coincide with those obtained analytically with

253    $N = +\infty$. Figure 1(c) shows the good agreement between SSL and RSL tensile flow stresses.

254   Thus, the yield stress and active slip systems are the same for both crystal plasticity laws

255   whereas the shear tangent moduli are different.

256

257   Following these comparisons at the single crystal level, the question which arises is the

258   influence, if any, of the different instantaneous local tangent moduli on the polycrystal

259   response. To tackle this problem, use will be made of the Taylor and self-consistent models

260   which are briefly described in the next section.

261

262   **3. Homogenization estimates**

263   *3.1. Self-consistent model*

264   In this study, we mainly focus on the role of the crystal plasticity law on the local and

265   effective response for the elastoplastic polycrystalline aggregate. Consequently, the Hill's

266   (1965) incremental self-consistent model, which is up to now the most widely used model for

267   elastoplastic polycrystal, is adopted. Polycrystal is considered to consist of ellipsoidal phases

268   which compose grains orientating at the same direction. In the self-consistent model, an

269   ellipsoidal phase is assumed to be embedded in an infinite linear comparison homogenous

270   medium which has a unique tangent moduli corresponding to the effective tangent ones. The

271   phase average stress and strain rates can be related to the macroscopic ones through the

272   localization tensors, $\mathbf{A}^r$ and $\mathbf{B}^r$,

273          $<\dot{\mathbf{\varepsilon}}>^r = \mathbf{A}^r : \dot{\bar{\mathbf{\varepsilon}}}, \quad <\dot{\mathbf{\sigma}}>^r = \mathbf{B}^r : \dot{\bar{\mathbf{\sigma}}},$ (30)

274   where the superscript r refers to the quantity for the r th phase, a bar indicates a

275   macroscopic value and $<\bullet>$ stands for a volume average. The rate-form constitutive

276   equation is used to represent linear relationship between the stress and strain rates. The

277   constitutive equations of a phase and effective medium are respectively denoted as

278          $<\dot{\mathbf{\sigma}}>^r = \mathbf{L}^r :<\dot{\mathbf{\varepsilon}}>^r,$ (31)

279          $\dot{\bar{\mathbf{\sigma}}} = \tilde{\mathbf{L}} : \dot{\bar{\mathbf{\varepsilon}}},$ (32)

280   with

281          $\tilde{\mathbf{L}} :=< \mathbf{L}^r : \mathbf{A}^r >.$ (33)

282   where $\mathbf{L}^r$ and $\tilde{\mathbf{L}}$ are the tangent moduli of a phase and effective medium, respectively. $\mathbf{L}^r$

283   is assumed to be homogeneous within a phase and can be calculated by Equation (15) or (24)

284   replacing the local quantities with the phase average ones, for instance, a resolved shear stress

285     $<\tau^{(\alpha)}>^r = \mathbf{p}^{(\alpha)} :< \mathbf{\sigma} >^r$ is used instead of $\tau^{(\alpha)} = \mathbf{p}^{(\alpha)} : \mathbf{\sigma}$. The strain localization tensor is given

286   by

287    $$\mathbf{A}^r = \{\mathbf{I} + \mathbf{P} : (\mathbf{L}^r - \tilde{\mathbf{L}})\}^{-1}.$$ (34)

288   where $\mathbf{I}$ is fourth-order identity tensor and $\mathbf{P}$ is so called Hill's tensor described as

289    $$\mathbf{P} = \int_\Omega \boldsymbol{\Gamma} \, dV ,$$ (35)

290   where

291    $$\Gamma_{ijkl} := \frac{1}{4}(K_{ik}^{-1}\xi_j\xi_l + K_{jk}^{-1}\xi_i\xi_l + K_{il}^{-1}\xi_j\xi_k + K_{jl}^{-1}\xi_i\xi_k) ,$$ (36a)

292    $$\mathbf{K} := \boldsymbol{\xi} \cdot \tilde{\mathbf{L}} \cdot \boldsymbol{\xi} ,$$ (36b)

293   where Ω is the domain within a phase and $\boldsymbol{\xi}$ is a position vector on the surface of

294   inclusion (see, for instance, Mura, 1982). This set of relations defines a nonlinear systems for

295   the average strain rates per phase, $<\dot{\boldsymbol{\varepsilon}}>^r$, which can be solved using a fixed-point iterative

296   algorithm.

297

298   *3.2. Taylor model*

299   In the Taylor model, $\mathbf{A}^r = \mathbf{I}$ is assumed, that is, the local strain field is taken to be identical

300   to the macroscopic one,

301    $$\dot{\boldsymbol{\varepsilon}} = <\dot{\boldsymbol{\varepsilon}}>^r = \bar{\dot{\boldsymbol{\varepsilon}}} .$$ (37)

302   Then, the effective tangent moduli in the rate-form of constitutive equation, $\bar{\dot{\boldsymbol{\sigma}}} = \tilde{\mathbf{L}} : \bar{\dot{\boldsymbol{\varepsilon}}}$, are

303   given by

304    $$\tilde{\mathbf{L}} = <\mathbf{L}> .$$ (38)

305   Since the local strain field is known a priori, iterative computation is not needed for the Taylor

306   model.

307

308   In the next section, the Taylor and incremental self-consistent models described above are

309   used in conjunction with SSL and RSL for estimating the mechanical behavior of f.c.c.

310   polycrystals at both local and overall scales.

311

312   **4. Results**

313   *4.1. Uniaxial tension for non-hardening f.c.c. polycrystalline aggregate*

314   Macroscopically isotropic polycrystal is considered. Its microstructure is represented by 216

315   crystalline phases with same volume fractions. Besides, a spherical shape is assumed for the

316   each phase. A non-hardening ($h^{\alpha\beta} = 0$) f.c.c. crystal with 12 slip systems, $\{111\} < 110 >$, is

317   assumed for each phase, and slip resistances are set as $g^{(\alpha)} = \tau_0$, where τ_0 is a critical

318   resolved shear stress. For simplicity isotropic elasticity with $E/\tau_0 = 1000$ and $\nu = 1/3$ is

319   considered. The exponent in the regularized Schmid laws is $N = 500$. (The effect of the

320   exponent, N, on homogenization estimates is discussed in Appendix.) Mechanical response

321   of the polycrystal subjected to the uniaxial tension in the x_1 direction is simulated with the

322   Taylor and self-consistent models in conjunction with the Schmid and regularized Schmid

323   laws.

324

325   Figure 2 shows the macroscopic uniaxial stress-strain curve, where the flow stress is

326   normalized by critical resolved shear stress, τ_0. For the Taylor model, the flow stresses

327   predicted by both the Schmid and regularized Schmid laws are in good agreement. Since

328    $N = 500$ is large enough, the regularized Schmid law approaches Schmid one as is

329   mentioned in section 2. The flow stresses, eventually, saturate to the value of 3.06, which is

330   the same as the well-known Taylor factor for rigid-plastic f.c.c. polycryatal.

331

332   For the self-consistent model, plastic yielding occur earlier than for the Taylor model and the

333   estimation of flow stress significantly depend on the crystal plasticity laws used in the

334   analysis. When the Schmid law is used, softer response is obtained. Indeed, the normalized

335   flow stress saturate to the value of 2.82. On the contrary, when the regularized Schmid law is

336   used, stiffer response is predicted and the stress state asymptotically approaches the one

337   predicted by the Taylor model. When the regularized Schmid law is used, the Taylor and

338   self-consistent models estimate almost the same behavior for the large strain range.

339

340   By definition, local strain states are the same as macroscopic one for the Taylor model and

341   vary for the self-consistent model. Figure 3 shows the evolution of local strain component

342 normalized by the macroscopic tensile strain for the self-consistent model. The normalized

343 strain components for 216 phases are depicted. During the whole tensile straining process, the

344 Schmid law based self-consistent model predicts about $\pm 15\%$ of constant variation of local

345 strain field. On the other hand, for the regularized Schmid law, similar variation is predicted

346 just after plastic yielding, but then the variation shrinks. At $\bar{\varepsilon}_{11} = 0.05$, the variation is less

347 than $\pm 2\%$. Thus, the self-consistent model with the regularized Schmid law is closer to the

348 Taylor model in terms of local field fluctuation. This small strain heterogeneity is consistent

349 with the macroscopic stress-strain curve that approaches the one of the Taylor model.

350

351 The local strain rate is specified by localization tensor in Equation (34), which includes the

352 local and effective tangent moduli and Hill's $\mathbf{P}$ tensor. The $\mathbf{P}$ tensor reflects the difference

353 of the local and effective tangent moduli to the localization tensor. The higher the components

354 of $\mathbf{P}$ are, the more enhanced the strain heterogeneity is. Components of $\mathbf{P}$ are shown in

355 Figure 4. For the Schmid model, the absolute value of the $\mathbf{P}$ components increase with

356 tensile straining. On the other hand, for the RSL, the $\mathbf{P}$ components are almost constant and

357 small. Therefore, the localization tensor is close to unit tensor and the fluctuation of local

358 strain field is small. The evolution of $\mathbf{P}$ tensor is in agreement with the local strain variation

359 in Figure 3.

360

361 As is shown in the equations (35) and (36), the $\mathbf{P}$ tensor depends on the effective tangent

362 moduli. Figure 5 shows the estimated effective tangent moduli in the rate-form of the

363 constitutive equations. The tangent moduli, $\tilde{L}_{ijkl}$, are normalized by the elastic moduli, C_{ijkl}^{e}.

364 For the uniaxial tensile loading, the macroscopic tangent moduli display transverse isotropy

365 with respect to the x_1 direction, that is, $\tilde{L}_{2222} = \tilde{L}_{3333}$, $\tilde{L}_{1122} = \tilde{L}_{1133}$ and $\tilde{L}_{1212} = \tilde{L}_{1313}$. The

366 tangent moduli predicted by the two crystal plasticity laws do not agree except for 1111 and

367 1122 components. Both tangent moduli depicted in Figure 5 correspond to uniaxial tension

368 state although they are not identical. The most significant difference is the shear tangent

369 moduli: those obtained with the Schmid law rapidly decrease after plastic yielding and

370 eventually reach to zero, whereas those for the regularized Schmid law are almost constant

371 during deformation. This trend is the same as that for the simple double slip case depicted in

372   Figure 1(b). General relationships between $\mathbf{P}$ and $\tilde{\mathbf{L}}$ are given in Equations (35) and (36)

373   and analytical expressions can be found by Hutchinson (1970) for transverse isotropic

374   symmetry. $\mathbf{P}$ tensor increases when $\tilde{\mathbf{L}}$ decreases, thus the lower $\tilde{\mathbf{L}}$ components

375   pronounce a deviation of the localization tensor from the identity tensor.

376

377   For the Taylor model, SSL and RSL give the identical behavior so long as the exponent is

378   high enough. However, for the self-consistent model, the description of the tangent moduli

379   affects the local strain heterogeneity as well as effective response.

380

381   *4.2. Polycrystalline aggregate with an elastic phase*

382   In this subsection, the polycrystal aggregate is assumed to consist of 216 elastoplastic phases

383   and an elastic phase. The elastic phase is considered in order to increase the contrast of the

384   mechanical properties among phases. The volume fraction of the elastic phase is 0.3 and that

385   of the other 216 phases are 0.00324. The material properties of the 216 elastoplastic phases

386   are the same as ones in 4.1, and the same elastic properties are assigned to an elastic phase.

387   All phases have spherical shape. Uniaxial tension in the x_1-direction is analyzed by means of

388   the self-consistent model. Taylor model is not used here because the uniform strain field

389   assumption is far from the reality for this problem.

390

391   Figure 6 shows the normalized flow stress as a function of the macroscopic tensile strain. The

392   Schmid law based model predicts softer response than that for the regularized Schmid law.

393   The qualitative tendency is the same as in Figure 2, and the existence of an elastic phase

394   enhances the difference of effective response. Figure 7 shows the local strain distribution of

395   the 216 elastoplastic and the elastic phases. The strain variation among the elastoplastic

396   phases is larger for the Schmid law than the regularized Schmid law. For the Schmid law, the

397   strain evolution in an elastic phase decreases with tensile strain, and the strain is much smaller

398   than that for the elastoplastic phases. On the other hand, for the regularized Schmid law the

399   strain develops linearly and its amount is about half of the elastoplastic phases. The Schmid

400   law allows lager strain heterogeneity among elastoplastic phases as well as between

401   elastoplastic and elastic phases. Figure 8 shows the effective shear tangent moduli normalized

402   by the same way as in 4.1. Again, the shear moduli decrease rapidly after yielding for the

403   Schmid law, whereas those for the regularized Schmid law are almost constant. The influence

404   of the tangent moduli emerges again for this problem and the strong contrast of the phases

405   enhances this effect on the local and effective response.

406

407   **5. Discussion**

408   The description of standard Schmid law and regularized Schmid law has been examined for a

409   uniaxial tensile loading (Section 2). It has become clear that both laws predict the same

410   mechanical behavior of single grain under given boundary conditions, provided that the

411   exponent in the regularized Schmid law is high enough. But, it has to be recalled that the

412   tangent moduli given by the two laws are different, although the same response is predicted.

413   For the non-hardening polycrystalline aggregate, the two laws with the Taylor model lead to

414   the same mechanical response under uniaxial tension. This can be explained by the fact that,

415   by definition, each phase undergoes the same strain field with the Taylor assumption. Since

416   the SSL and RSL predict the same response for a phase under the same boundary conditions,

417   the same mechanical response is predicted for each phase and consequently, the same local

418   and effective responses are obtained for the polycrystal.[2] On the other hand, the two crystal

419   plasticity laws lead to different estimates with the incremental self-consistent model. The

420   shear tangent moduli for the SSL are lower than those for the RSL and are used to obtain

421   strain localization tensors which specify the average strain field within a phase. Therefore,

422   with the self-consistent model, the average strain field of a given phase varies between the

423   SSL and RSL. Furthermore, the lower the tangent moduli are, the more the strain

424   heterogeneity is enhanced. As a consequence, the self-consistent model with the SSL leads to

425   the larger strain heterogeneity and softer overall response. On the other hand, the

426   self-consistent model with the RSL predicts a smaller strain heterogeneity and a flow stress

427   approaching to the upper bound. From this point of view, it can be concluded that the

428   self-consistent model based on the SSL gives a better estimation.

---

[2] Uniaxial tensile behavior is also computed for the static model, which assumes a uniform stress field within the polycrystal. SSL and RSL with $N = 500$ estimate the same behavior and the macroscopic stress is stationary at $\bar{\sigma}_{11} / \tau_0 = 2$.

429

430   There are some similarities in the constitutive equations for the RSL and a power law

431   viscoplasticity model: (i) the slip law in equation (19) and the one for viscoplascity both obey

432   a power law, (ii) the regularized Schmid law possesses a smooth yield locus and the

433   viscoplastic model presents a smooth equal potential locus in stress space. The power law

434   viscoplastic model can thus also be considered as a regularization of the Schmid law.

435   Numerous investigations have been performed on the self-consistent model in the viscoplastic

436   context (see, among others, Hutchinson, 1976; Masson et al., 2000; Nebozhyn et al., 2001)

437   and it has been shown that the effective yield stress predicted by the Hill's incremental model

438   in the rate-independent limit is very close to the Taylor bound. By noting that this effective

439   yield stress corresponds to the saturated flow stress of a non-hardening elastoplastic

440   polycrystal, it is pointed out that our self-consistent estimates with a RSL are fully consistent

441   with the results obtained in the viscoplastic context. Following these remarks, it is likely that

442   any regularization (i.e. single yield function with associated flow rule) would lead to

443   incremental self-consistent estimates with the same shortcomings than the one reported in the

444   present study.

445

446   The physical interpretation of the reduced shear tangent moduli is considered here. First, a

447   situation is assumed such that the double slip single grain shown in Figure 1(a) is

448   continuously subjected to the uniaxial tension, and instantly shear strain rate, $\dot{\varepsilon}_{12}$, is applied

449   additionally. Schematic illustration of yield surfaces for the RSL and SSL in $\sigma_{11} - \sigma_{12}$ space

450   are shown in Figure 9. In these circumstances, the stress state is uniaxial tension, i.e. $\sigma_{ij} = 0$

451   except for σ_{11}, and non-zero strain rate components are $\dot{\varepsilon}_{11}$, $\dot{\varepsilon}_{22}$ and $\dot{\varepsilon}_{12}$. For the RSL, the

452   direction of the plastic strain rate is normal to the yield surface at the current stress state and

453    $\dot{\varepsilon}_{12}^{\mathrm{p}}$ is not produced, hence $\dot{\varepsilon}_{12}$ is accomplished by elastic strain rate, $\dot{\varepsilon}_{12}^{\mathrm{e}}$. Thus, the tangent

454   modulus of L_{1212} is identical to the elastic shear modulus. On the other hand, for the RSL,

455   the direction of plastic strain rate lies between the normal directions of the facets. Therefore,

456   when $\dot{\varepsilon}_{12}$ is applied, $\dot{\varepsilon}_{12}^{\mathrm{p}}$ is produced and the tangent modulus is consequently reduced. The

457   introduction of the regularization, which avoids the difficulty of the selection of active slip

458   systems, loses the vertex effect on the tangent moduli.

459

460   It is interesting to note an analogy between the standard and regularized Schmid laws and the

461   phenomenological J_2 flow and J_2 deformation theories. Reduced tangent moduli were

462   observed by Hutchinson (1970) who compared tangent moduli for the J_2 flow and

463   deformation theories. The flow theory assumes a smooth yield locus and associated flow rule

464   and the deformation theory reflects the point vertex effect on the yield surface. The flow and

465   deformation theories predict respectively constant and decreasing shear tangent moduli during

466   plastic deformation. The flow and deformation theories are similar to the RSL and SSL,

467   respectively. In fact, there is a vertex on the yield locus for the SSL and a single smooth yield

468   locus and associated flow rule are assumed in the RSL (Equations (16) and (18)).

469

470   In the crystalline context, our results highlight the fact that the flow stress estimate obtained

471   with a regularized crystal plasticity law can be different from the one that is obtained with the

472   non-smooth multi-criteria yield function corresponding to the SSL. In particular, the

473   incremental self-consistent model is significantly affected by the mathematical description of

474   the constitutive model and does not always lead to a stiff overall response with respect to the

475   Taylor model. Indeed, with the incremental self-consistent model, the Schmid law gives a

476   saturated flow stress of 2.82, which is lower than the estimation derived from the viscoplastic

477   power law in the rate-independent limit (≈ 3.06). Interestingly, it is noted that the saturated

478   flow stress obtained with the SSL does not violate the variational self-consistent estimate of

479   Ponte Castañeda for viscoplastic behavior which is equal to 2.948 in the rate-independent

480   limit (Nebozhyn et al. 2001). To give an insight on the pertinence of Hill's incremental model

481   in the framework of the standard Schmid law, it would be necessary to compare the

482   self-consistent estimate of the saturated flow stress with more rigorous bounds: the one

483   derived for polycrystalline materials exhibiting a rigid-plastic behavior with a multi-criteria

484   local yield function (see, for instance, Nesi et al., 2000) or the recent improvement of the

485   variational approach of Ponte Castañeda (Idiart and Ponte Castañeda 2007a,b) which was

486   shown to improve on earlier bounds in the case of a two-phase porous crystalline material.

487

488   Concerning the RSL, it is interesting to note that different studies on particulate composites

489   (matrix-inclusion microstructure) (Gonzales and LLorca, 2000; Doghri and Ouaar, 2003;

490   Chaboche et al., 2005) with an elastoplastic matrix obeying the J_2 flow theory have shown

491   that the incremental model deliver a too stiff overall stress-strain response by comparison with

492   finite element computations. This is qualitatively in agreement with our results obtained by

493   RSL for non-hardening polycrystal with an elastic phase. To obtain better self-consistent

494   estimates, it would be necessary to incorporate the field heterogeneity in the nonlinear

495   homogenization procedure for elastoplasticity.

496

497   6. Concluding remarks

498   The mechanical response of polycrystals has been investigated using the Hill's incremental

499   self-consistent model in conjunction with different rate-independent crystal plasticity laws.

500   The investigation of standard and regularized Schmid laws has revealed that they deliver the

501   same plastic deformation behavior but different tangent moduli. The use of these two

502   constitutive laws to describe the elastoplastic behavior of a non-hardening f.c.c. polycrystal

503   has shown that the standard Schmid law predicts a wider heterogeneity of the local strain field

504   and a softer overall response. We found that the reduced shear tangent moduli are responsible

505   for this behavior. The incorporation of an elastic phase in the elastoplastic polycrystal allowed

506   us to point out that an increase of the mechanical contrast implies a more pronounced

507   influence of the tangent moduli on the self-consistent description. The shear tangent moduli

508   decrease with the deformation for the SSL and remain constant for the RSL. With the

509   incremental self-consistent model, the Schmid law gives a saturated flow stress which is

510   lower than the estimation derived from the viscoplastic power law in the rate-independent

511   limit. The saturated flow stress obtained with the SSL (Hutchinson, 1970) does not violate the

512   variational self-consistent estimate of Ponte Castañeda for viscoplastic behavior in the

513   rate-independent limit. Comparisons with more restrictive bounds are thus required.

514

515   7. Acknowledgements

517

8. References

518

519 Anand, L., and Kothari, M., 1996. A computational procedure for rate-independent crystal

520   plasticity. Journal of the Mechanics and Physics of Solids, 44(4), 525-558.

521 Asaro, R., and Needleman, A., 1985, Texture development and strain hardening in rate

522   dependent polycrystals. Acta Metallurgica 33(6), 923-953.

523 Bassani, J.L., 1994. Plastic flow of crystals. In: Advances in Applied Mechanics, Volume 30.

524 Academic Press, London, pp. 191-258.

525 Brenner, R., Lebensohn, R. A., Castelnau O., Elastic anisotropy and yield surface estimates of

526   polycrystals, submitted.

527 Budiansky, B., Hashin, Z. and Sanders, J. L., 1960. The stress field of a slipped crystal and the

528   early plastic behavior of polycrystalline materials Plasticity. In: Proceedings of the 2nd

529   Symp Naval Struct Mech., Pergamon, Oxford, 1960, 239.

530 Busso, E. P. and Cailletaud, G., 2005. On the selection of active slip systems in crystal

531   plasticity. Internatinal Journal of Plasticity 21(11), 2212-2231.

532 Castelnau, O., Brenner, R. and Lebensohn, R.A., 2006. The effect of strain heterogeneity on

533   the work hardening of polycrystals predicted by mean-field approaches. Acta Materialia,

534   54(10) 2745-2756.

535 Chaboche, J.L., Kanoute, P., Roos A., 2005. On the capabilities of mean-field approaches for

536   the description of plasticity in metal matrix composites. International Journal of

537   Plasticity 21 (7) 1409-1434.

538 Darrieulat, M., Piot, D., 1996. A method of generating analytical yield surfaces of crystalline

539   materials. International Journal of Plasticity 12(5) 575-610.

540 Doghri, I., Ouaar, A., 2003. Homogenization of two-phase elasto-plastic composite materials

541   and structures, Study of tangent operators, cyclic plasticity and numerical algorithms.

542   International Journal of Solids and Structures 40 (7) 1681-1712.

543 Franciosi, P. and Berbenni, S., 2007. Heterogeneous crystal and poly-crystal plasticity

544   modeling from a transformation field analysis within a regularized Schmid law. Journal

545   of the Mechanics and Physics of Solids, 55(11) 2265-2299.

546 Franciosi, P. and Zaoui A., 1991. Crystal hardening and the issue of uniqueness. International

547   Journal of Plasticity, 7(4) 295-311.

548   Franz, G., Abed-Meraim, F., Lorrain, J.-P., Ben Zineb T., Lemoine, X. and Berveiller, M.,

549   2009. Ellipticity loss analysis for tangent moduli deduced from a large strain

550   elastic–plastic self-consistent model, International Journal of Plasticity, 25(2) 205-238.

551   Gambin, W., 1992. Refined analysis of elastic-plastic crystals, International Journal of Solids

552   and Structures 29 (16) 2013-2021.

553   Gambin, W., Barlat, F., 1997. Modeling of deformation texture development based on rate

554   independent crystal plasticity. International Journal of Plasticity 13(1-2) 75-85.

555   Gonzalez, C., LLorca, J., 2000. A self-consistent approach to the elasto-plastic behaviour of

556   two-phase materials including damage. Journal of the Mechanics and Physics of Solids

557   48 (4) 675-692.

558   Hershey, A.V., 1954. The elasticity of an isotropic aggregate of anisotropic cubic crystals,

559   Journal of Applied Mechanics, 21(9) 236-240

560   Hill, R., 1965. Continuum micro-mechanics of elastoplastic polycrystals. Journal of the

561   Mechanics and Physics of Solids, 13(2) 89-101.

562   Hill, R. 1966. Generalized constitutive relations for incremental deformation of metal crystals

563   by multislip. Journal of the Mechanics and Physics of Solids, 14(2), 95-102.

564   Hutchinson, J.W., 1970. Elastic-plastic behaviour of polycrystalline metals and composites.

565   Proceedings of the Royal Society of London A 319(1537) 247-272.

566   Hutchinson, J.W., 1976. Bounds and self-consistent estimates for creep of polycrystalline

567   materials. Proceedings of the Royal Society of London A 348(1652) 101-127.

568   Idiart, M.I. and Ponte Castañeda, P., 2007. Variational linear comparison bounds for nonlinear

569   composites with anisotropic phases. I. General results. Proceedings of the Royal Society

570   A, 463(2080), 907-924.

571   Idiart, M.I. and Ponte Castañeda, P., 2007. Variational linear comparison bounds for nonlinear

572   composites with anisotropic phases. II. Crystalline materials. Proceedings of the Royal

573   Society A, 463(2080), 925-943.

574   Kowalczyk, K. and Gambin, W., 2004. Model of plastic anisotropy evolution with

575   texture-dependent yield surface Int. J. Plasticity, 20(1), 19-54.

576   Kröner, E., 1958, Berechnung der elastischen Konstanten des Vielkristalls aus den Konstanten

577   des Einkristalls Z. Physik, 151, 504-518.

578 Kröner, E., 1961. Zur plastischen Verformung des Vielkristalls. Acta Metallurgica, 9(2)
579   155-191.

580 Kröner, E., 1978. Self-consistent scheme and graded disorder in polycrystal elasticity. Journal
581   of Physics F: Metal Physics, 8(11), 2261-2267.

582 Lebensohn, R.A., Liu, Y. and Ponte Castañeda, P., 2004. On the accuracy of the
583   self-consistent approximation for polycrystals: comparison with full-field numerical
584   simulations, Acta Materialia, 52(18) 5347-5361.

585 Masson, R., Bornert, M., Suquet, P. and Zaoui, A., 2000. An affine formulation for the
586   prediction of the effective properties of nonlinear composites and polycrystals. Journal of
587   the Mechanics and Physics of Solids 48(6-7), 1203-1227.

588 Miehe, C. and Schröder, J., 2001. A comparative study of stress update algorithms for
589   rate-independent and rate-dependent crystal plasticity. International Journal for
590   Numerical Methods in Engineering 50(2)273-298.

591 Mura, T, 1982, Micromechanics of defects in solids. Martinus Nijhoff Publishers, The Hague.

592 Nebozhyn, M. V., Gilormini, P. and Ponte Castañeda, P., 2001. Variational self-consistent
593   estimates for cubic viscoplastic polycrystals : the effects of grain anisotropy and shape.
594   Journal of the Mechanics and Physics of Solids, 49(2), 313-340.

595 Nesi, V., Smyshlyaev, V.P. and Willis J.R., 2000. Improved bounds for the yield stress of a
596   model polycrystalline material. ournal of the Mechanics and Physics of Solids 48(9),
597   1799-1825.

598 Ponte Castañeda, P., 1991. The effective mechanical properties of nonlinear isotropic
599   composite. Journal of the Mechanics and Physics of Solids, 39(1), 45-71.

600 Takahashi, H., 1988. Predictions of plastic stress-strain relations of polycrystals based on the
601   Lin model. International Journal of Plasticity, 4(3), 231-250.

602

603 **Appendix**

604 *A1. Influence of exponent, N, in regularized Schmid law*

605 The exponent, N , in the regularized Schmid law has been taken to 500 for the all

606 computations in Section 4. In this section, N is taken to 5 and 50 in order to examine its

607 influence on the microscopic and macroscopic mechanical responses, and the problems in

608   Section 4.1 and 4.2 are simulated. Figure A1(a) shows the macroscopic uniaxial stress-strain

609   curve for the isotropic non-hardening crystalline aggregate. The saturated flow stresses

610   predicted with the Taylor and self-consistent models coincide with each other for the same

611   N and decrease with N. When $N = 5$, the flow stresses predicted by the Taylor and

612   self-consistent models are softer than the one predicted by the self-consistent model with the

613   Schmid law (Figure 2), since the yield stress of a single crystal becomes lower with

614   decreasing the exponent. Thus, this prediction does not imply that the regularized Schmid law

615   with $N = 5$ is capable of predicting the softer effective response with large strain

616   heterogeneity. The development of the phase average strain for $N = 5$ is shown in Figure

617   A1(b). The phase average strains once have a variation in the range of -20% to +10% just

618   after the plastic yielding and then, the variation shrinks. The amount of strain heterogeneity is

619   the same magnitude as the one for $N = 500$ in Figure 3(b). The strain heterogeneity for

620    $N = 50$, which is not shown in the present paper, is almost the same as that for $N = 500$.

621   Therefore, it is concluded that the exponent, N, has little influence on the estimation of

622   mechanical response.

623

624   The microscopic and macroscopic deformation of polycrystals reinforced by an elastic

625   inclusion, which is the problem in Section 4.2, is also simulated for $N = 5$ and 50, and the

626   results are shown in Figure A2. Softer behavior is predicted for the case of $N = 5$, since lower

627   exponent gives softer flow stress for a single crystal. Figure A2(b) shows the strain

628   distribution in the polycrystalline and elastic phases. The predicted strain heterogeneity is

629   almost the same as the one for $N = 500$ shown in Figure 7(b). We again conclude that the

630   exponent, N, in the regularized Schmid law has almost no influence on the estimation of the

631   mechanical behavior.

632

1   (a)

2   (b)


3   (c)
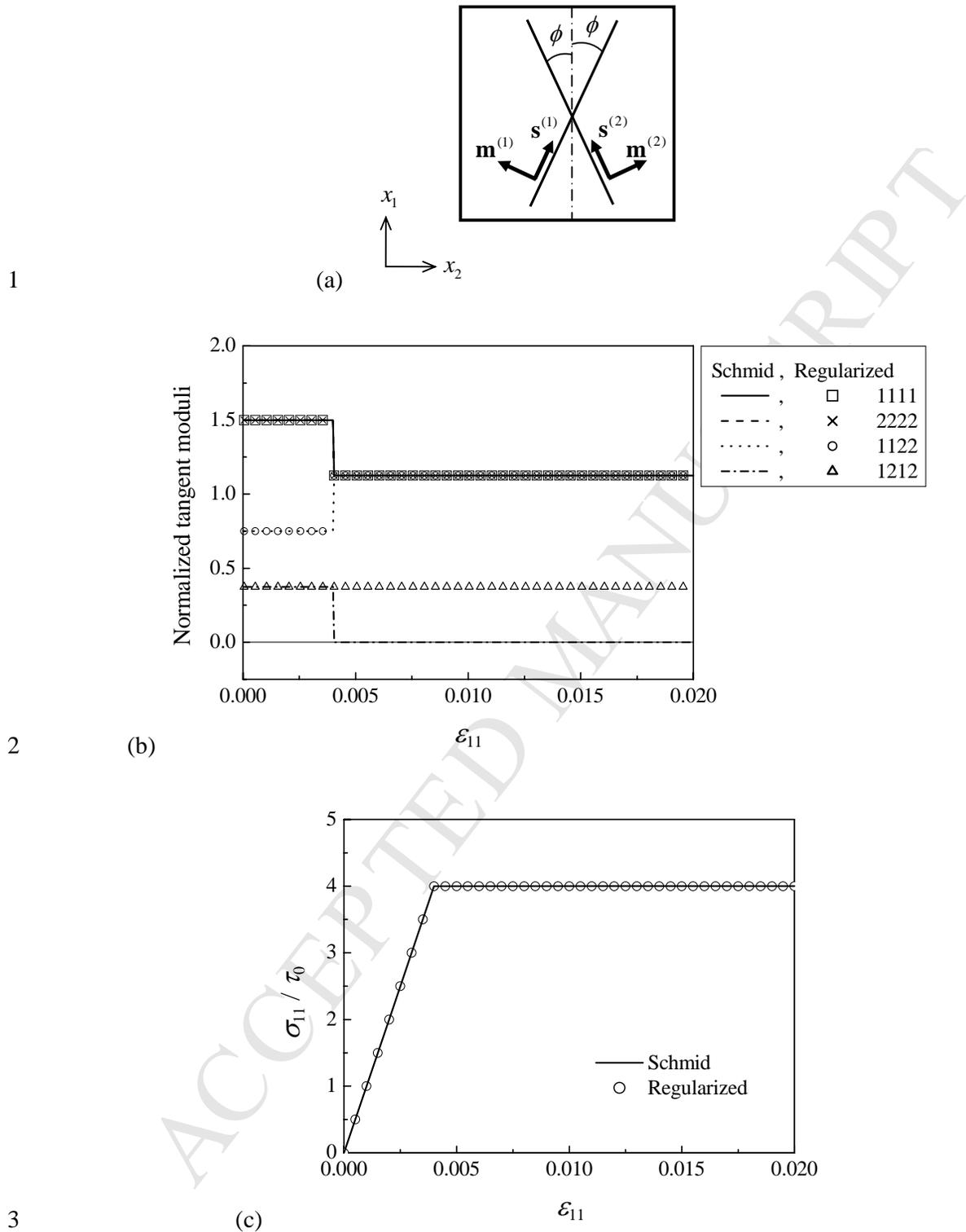
4   Figure 1.   Tangent moduli for a double slip crystal under uniaxial tension. (a) Geometry of

5   slip systems, (b) tangent moduli normalized by the Young's modulus and (c) tensile stress

6   normalized by a critical resolved shear stress as a function of tensile strain.
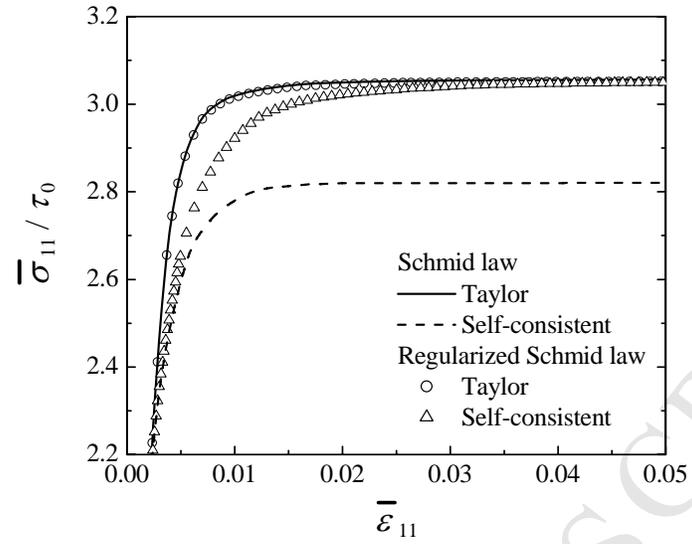
7

8   Figure 2.   Macroscopic uniaxial stress-strain curve for isotropic non-hardening f.c.c.

9   crystalline aggregate. Taylor and incremental self-consistent models are used in conjunction

10   with Schmid and regularized Schmid laws.
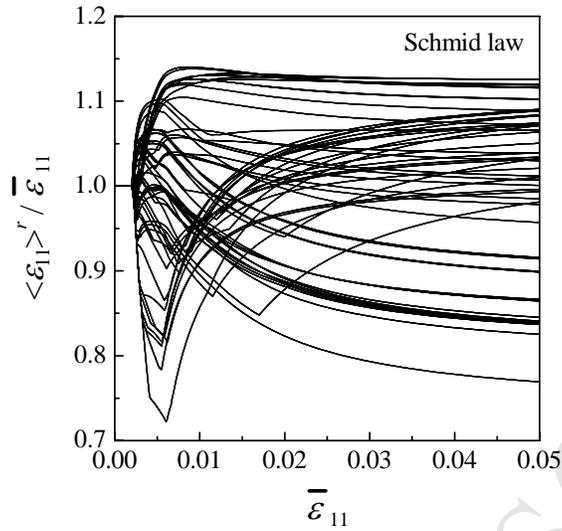
(a)
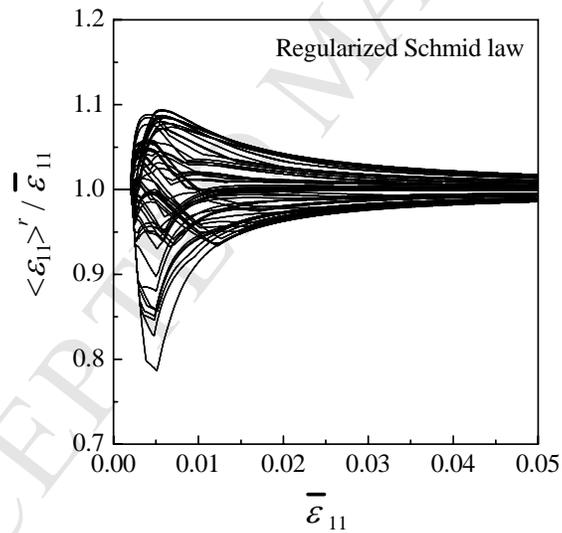
(b)

Figure 3.   Evolution of local strain component, $< \varepsilon_{11} >^r$, in 216 phases under uniaxial tension. Incremental self-consistent model is used in conjunction with (a) Schmid law and (b) regularized Schmid law.

$(\times 10^{-4})$

(a)

$(\times 10^{-4})$

(b)
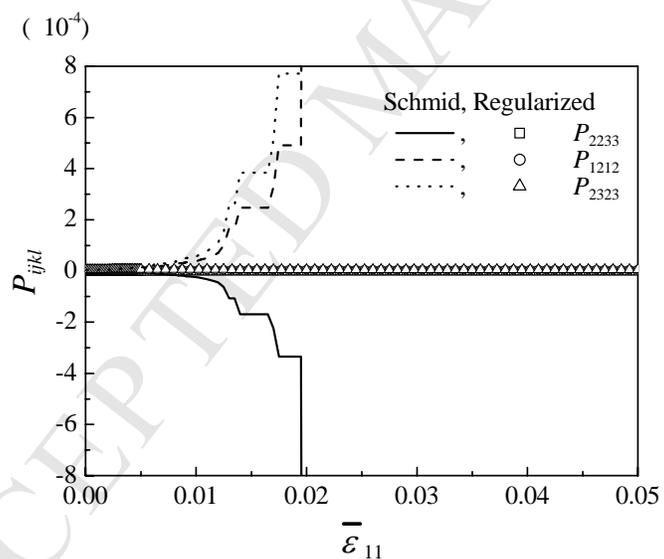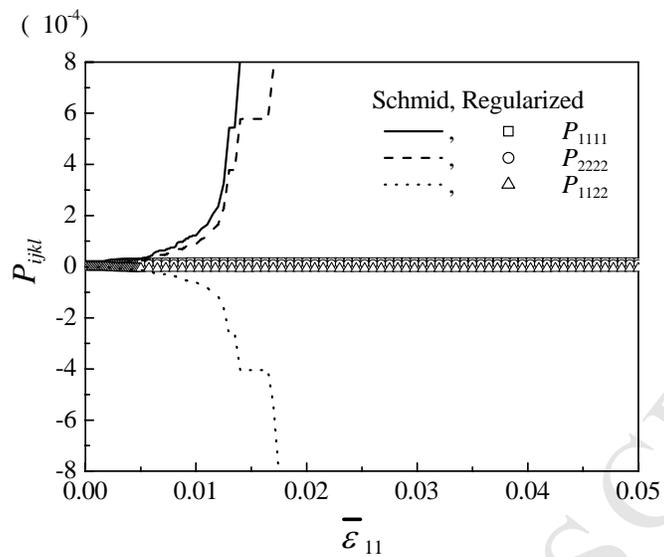
Figure 4. Evolution of **P** tensor for uniaxial tension as a function of macroscopic tensile strain.

28
29   (a)
30
31

32
33   (b)
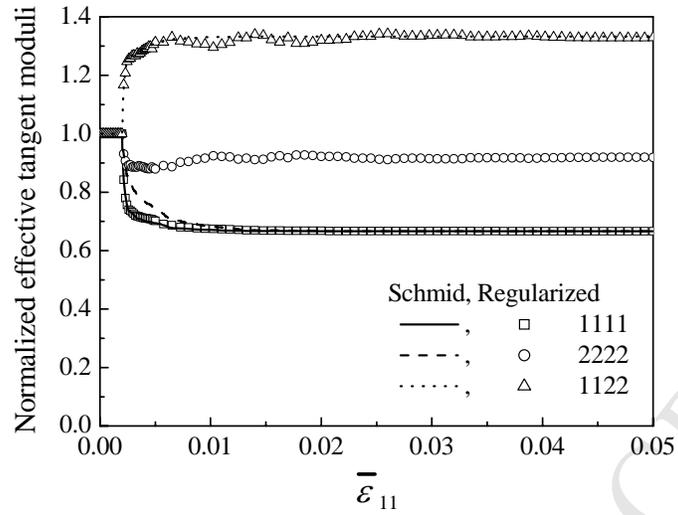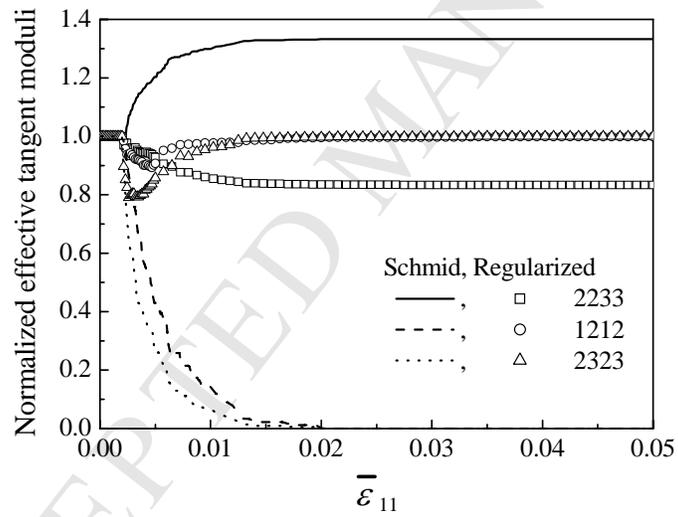
34   Figure 5.   Evolution of tangent moduli under uniaxial tension. Effective tangent moduli,

35                $\tilde{L}_{ijkl}$, are normalized by corresponding elastic moduli, C_{ijkl}^{e} .
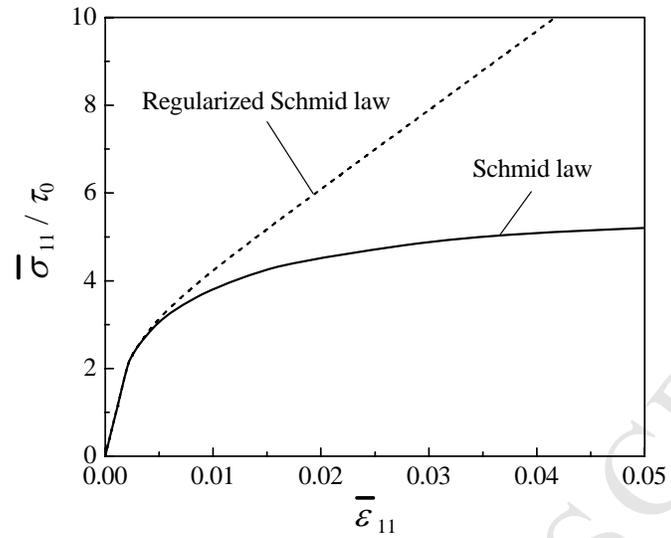
36

37   Figure 6.   Stress-strain curve for aggregate consisting of elastoplastic phases and an elastic

38   phase. Incremental self-consistent model is used in conjunction with Schmid and regularized

39   Schmid laws.

40

41   (a)

42

43

44

45   (b)
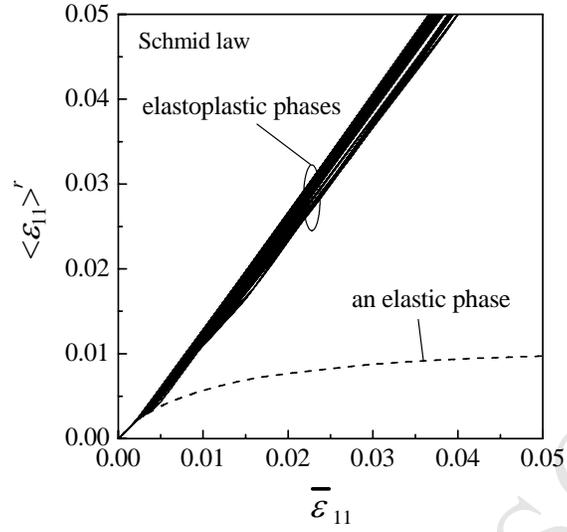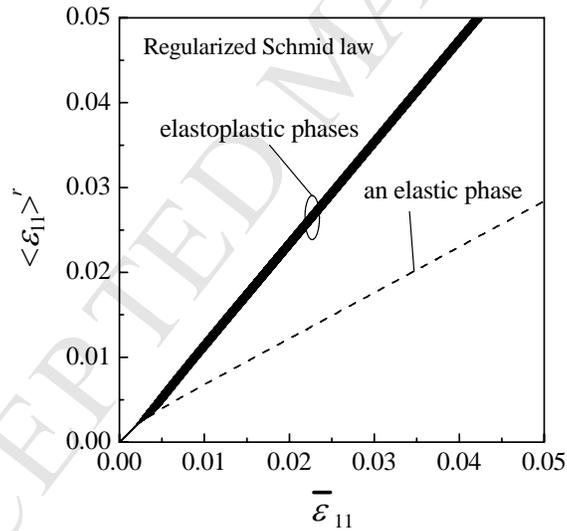
46   Figure 7.   Evolution of local strain component, $< \varepsilon_{11} >^r$, in 216 elastoplastic phases and an

47   elastic phase under uniaxial tension. Incremental self-consistent model is used in conjunction

48   with (a) Schmid law and (b) Regularized Schmid law.

49

50   Figure 8.   Evolution of tangent moduli for aggregate consisting of 216 elastoplastic phases

51   and an elastic phase under uniaxial tension. Effective tangent moduli, $\tilde{L}_{ijkl}$, are normalized by

52   elastic moduli, C_{ijkl}^{e} , for each component.

53
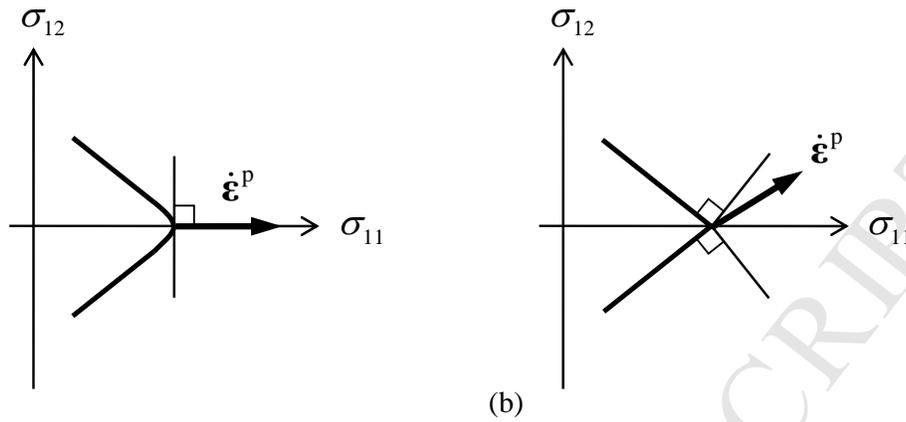

54   (a)   (b)

55   Figure 9.   Schematic illustration of yield surface in $\sigma_{11} - \sigma_{12}$ space based on (a) regularized

56   and (b) standard Schmid laws for a double slip crystal shown in Figure 1.

57

58   (a)

59

60

61   (b)
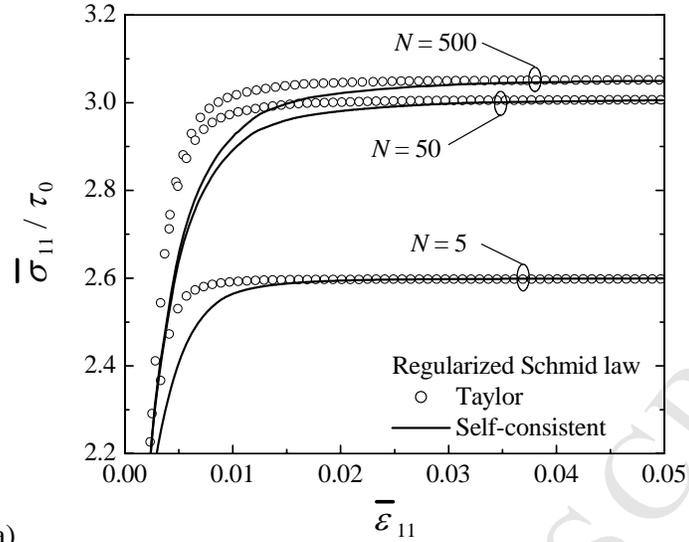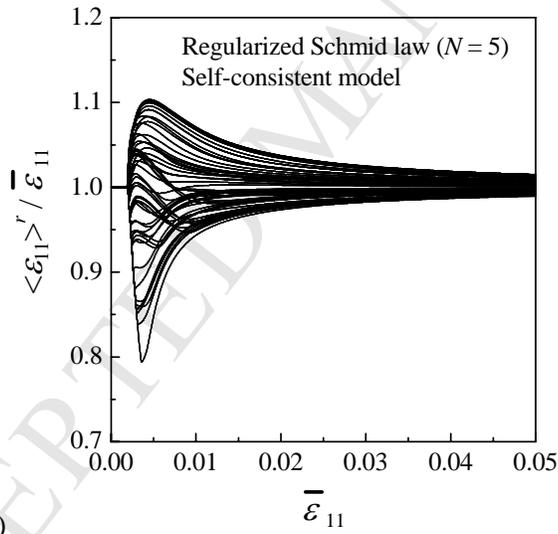
62 Figure A1. Influence of exponent in regularized Schmid law for isotropic non-hardening

63   f.c.c. polycrystal. (a) Macroscopic flow stress and (b) strain heterogeneity.

64   (a)

65

66

67   (b)
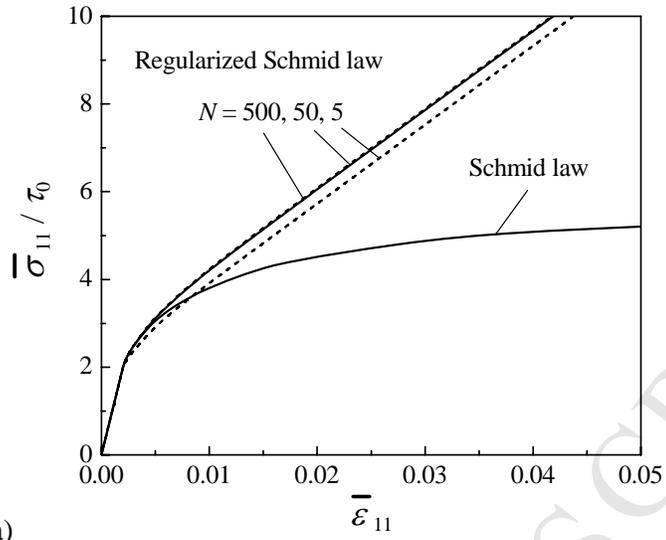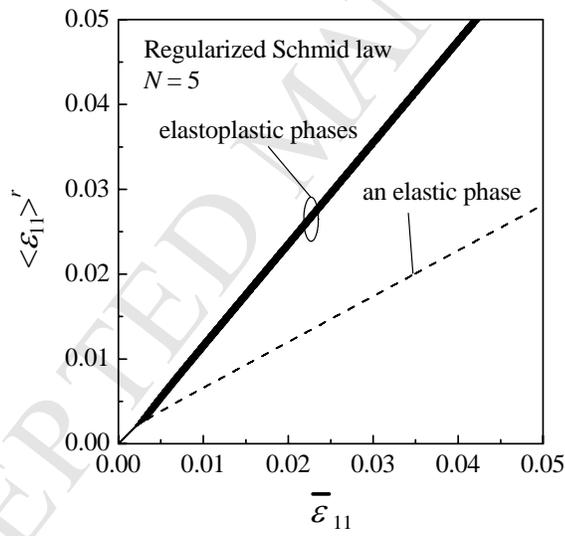
68   Figure A2.   Influence of exponent in regularized Schmid law for isotropic non-hardening

69 f.c.c. polycrystal reinforced by an elastic inclusion. (a) Macroscopic flow stress and (b) strain

70   heterogeneity.

71